Shifted thermal extraction rates in large Borehole Heat Exchanger array - a numerical experiment

Shuang Chen[a,b], Francesco Witte[c], Olaf Kolditz[a,b], Haibing Shao[a,d]

[a]*Helmholtz Centre for Environmental Research – UFZ, 04318 Leipzig, Germany*
[b]*Dresden University of Technology, 01069 Dresden, Germany*
[c]*Flensburg University of Applied Sciences, 24943 Flensburg, Germany*
[d]*Freiberg University of Mining and Technology – TUBAF, 09599 Freiberg, Germany*

Abstract

In large scale Ground Source Heat Pump (GSHP) systems, multiple Borehole Heat Exchangers (BHEs) are often connected with the pipe network array to extract shallow geothermal energy. In this study a comprehensive numerical model was developed. The heat transport within and around the BHEs and the pipe network is explicitly quantified in a coupled manner. The model allows a dynamic heat extraction calculation on the individual BHE that is determined by the hydro-thermal processes in the pipe network. The model is thus capable of capturing the long-term thermal interference among BHEs. The model was verified against analytical solution with respect to its hydraulic and thermal balances. Based on it, a series of numerical experiments have been performed to quantitatively investigate the amount of shifted thermal extraction rate in large BHEs array. It is found that, the heat extraction rate on the central BHEs was gradually shifted towards those located at the edge in the long-term operation. Over different seasons, the strongest shifting phenomenon was observed in the month with the lowest thermal load. The shift becomes significant with the increasing number of BHEs installed. The result of numerical study suggests that traditional super-positioned based infinite line source approach with a constant heat flux is not accurate enough for long-term prognosis since it does not fully consider the thermal recharge and the thermal interference effects.

Keywords: Shallow geothermal energy extraction, Ground Source Heat Pump (GSHP), Borehole Heat Exchanger (BHE) array, Shifted heat extraction rate, OpenGeoSys (OGS), Thermal Engineering Systems in Python (TESPy).

Nomenclature

Roman letters

a	proportion of the shifted thermal load over the mean load value (%)
c	specific heat capacity (J Kg^{-1} K^{-1})
D	diameter of the pipe (m)
E_1	exponential integral function
H	thermal sink/source term (W m^{-3})
h	enthalpy of circulating fluid ($J\ kg^{-1}$)
k_s	roughness coefficient of the pipe (m)
$\dot{m}$	flow rate of circulating fluid (kg s^{-1})
N_{dof}	number of degrees of freedom
P	power of the pipe network component (W)
p	hydraulic pressure of circulating fluid (Pa)
$\dot{Q}$	heat extraction rate of the BHE (W)
$q_{\mathrm{k,l}}$	sequence of heat extraction pulses (W)
q_n	heat flux between soil, grout and pipe (W m^{-2})
Re	Reynolds number ($-$)
T	temperature (°C)
t	time (s)
$\mathbf{u}$	velocity vector of circulating fluid (m s^{-1})
$\mathbf{v}$	Darcy velocity vector of groundwater flow (m s^{-1})

v Flow velocity in pipelines (m s^{-1})

Greek Letters

α soil thermal diffusion coefficient (W m^{-1} K^{-1})

ϵ numerical error ($-$)

η viscosity of circulating fluid ($kg\ m^{-1}\ s^{-1}$)

Γ domain boundary

Λ hydrodynamic thermal dispersion tensor (W m^{-1} K^{-1})

λ thermal conductivity (W m^{-1} K^{-1})

Ω domain ($-$)

ϕ heat transfer coefficient (W m^{-2} K^{-1})

π mathematical constant Pi ($-$)

ρ density (kg m^{-3})

ε volume fraction, porosity ($-$)

ζ friction factor of the pipe in Eq. (5) ($-$)

Operators

Δ difference operator

∇ spatial gradient operator

$\nabla\cdot$ spatial divergence operator

Subscripts

dof degrees of freedom

f fluid

g grout

i pipe-in or internal

o pipe-out or outer

Superscripts

$1U$ single U-shape pipe

f fluid

g grout

r circulating fluid (refrigerant)

s solid or soil

Abbreviations

$1U$ single U-shape pipe

BHE borehole heat exchanger

COP coefficient of performance

$GSHP$ ground source heat pump

1. Introduction

In the first decade of this century, the global installed geothermal heating and cooling applications have been increasing with a growing momentum [1, 2]. Among the different technology options, utilising geothermal energy through Ground Source Heat Pump (GSHP) system has the most significant impact. It has the largest installed capacity worldwide (70.90%) and growing at a compound rate of 10.3% since 2010 [3]. A recent trend in the industry is to build large GSHP system targeting commercial buildings and small neighbourhood [4], where dozens, in some cases hundreds of Borehole Heat Exchangers (BHEs), were connected with a pipe network to form a BHE array in order to supply the higher thermal load for large buildings. Especially in urban areas where the land is limited, this type of shallow geothermal exploitation is often favourable, because the accelerated heat fluxes between the warmed basement often leads to elevated temperatures in the urban subsurface [5, 6, 7].

For the design of such BHE arrays, various analytical and numerical models have been developed. Firstly, Eskilson [8] presented the super-position borehole model to estimate the soil temperature distribution induced by infinite line source. This model contains the well known g-functions representing the non-dimensional thermal response deduced by an instantaneous thermal load. The method was further improved by Bernier et al. [9] by considering the past steps thermal response effect to the current temperature distribution. Using this super-position principle, several analytical solutions are further developed. Lamarche and Beauchamp [10] demonstrated a mathematical algorithm which is not dependent on the previous step thermal response. Koohi-fayegh and Rosen [11] analyzed the two neighbouring boreholes and then further developed a more accurately analytical approach considered the thermal interference among BHEs that are connected in an array [12]. Qian and Wang [13] presented a model to investigate the relationship between the soil temperature distribution and the Coefficient of Performance (COP) of the heat pump. Based on the finite line source model, Rivera et al. [14] presented a semi-analytical approach which could estimate the transient temperature distribution in a three-dimensional domain. For the seasonal heating and cooling strategy in a multi-BHE array, Bayer et al. [15] developed a mathematical procedure also based on super-position principle to optimise the BHE field operation. Zhang et al. [16] summarised the most typical computational methods for ground dynamic thermal response.

On the other hand, numerical models targeting BHEs array design are making considerable advances in recent years, since they have the advantages in simulating the complex subsurface conditions that cannot be reliably calculated by analytical models. The well known Duct Storage model is widely applied in the design and analysis of underground energy storage system [17]. Morrone et al. [18] investigate the long term behaviour of an energy pile system with numerical simulator PILESIM2 [19]. Similar to the Duct Storage model, the PILESIM2 simulator aggregates all the heat exchanger piles into a store cylinder volume, by which the heat transfer between each BHE and the surrounding soil is not explicitly quantified. Lee and Lam [20] presented a three-dimensional model for a single cylindrical energy pipe. Koohi-fayegh and Rosen [11] proposed a numerical model to investigate the thermal behaviour between two boreholes considering their possible thermal interference. Hein et al. [21] investigate the soil temperature evolution induced by a configuration of four individual GSHP systems. Saaly et al. [22] built a numerical 3D heat absorber panel model with the software COMSOL Multiphysics [23] to investigate the effect of heat loss in a building which was equipped with an geothermal energy pile system in Canada. Hénault et al. [24] simulated a hybrid ground-coupled heat pump system which could significantly reduce the electrical consumption of a building.

In the above mentioned analytical and numerical approaches, the heat extraction rate on each BHE is mostly defined as an imposed boundary condition and the surrounding soil temperature distribution is assumed to be in an equilibrium state to satisfy that. These assumptions hold true for a single BHE, but it may deviate from the reality when the thermal plumes from neighbouring BHEs are interfering with each other. In heating applications, the overlapping thermal plumes can lead to low temperature zones in the centre of the BHE array, indicating a thermal imbalance in the subsurface [4, 7]. This imbalance may further lower the thermal extraction rate on the individual BHE, depending on where it is located. To quantify such interference, several analytical approaches have been developed. The well-known ASHRAE method [25] adopts the concept of temperature penalty to estimate the long-term ground temperature changes with explicit consideration of soil thermal imbalances. Being aware of the different heat extraction rates, Gultekin et al. [26] further extended his analytical formulation, in which the individual extraction rate is dependent on the number of BHEs and the spacing between them. Witte [27] presented a simple diagram to assess the change of soil temperature in the vicinity of a BHE based on the distance to the next borehole and the thermal load imposed on it. You et al. [28] also proposed a coupled analytical approach, in which the heat extraction rate of each energy pile is coupled with the groundwater flow velocity, the depth of BHEs, as well as the spacing between them.

Despite of these developments, the modelling approaches mentioned above are limited in describing several important physical processes. Firstly, the thermal recharge is not considered in most of the analytical solutions. The seasonal surface temperature fluctuation at the ground surface and the vertical geothermal gradient contribute to the thermal recharge of shallow subsurface [29, 30, 31]. Without the quantification of thermal recharge, the long-term thermal imbalance in the subsurface cannot be accurately predicted and may lead to deviated results especially for the prognosis over 10 to 20 years. Secondly, most analytical approaches are based on the principle of super-position to calculate the change of dimensionless soil temperature. Over the long operation period, the groundwater flow velocity and the hydraulic condition around each BHE are always time-dependent. This makes it difficult to calculate the dimensionless soil temperature change. Thirdly, in most analytical and numerical approaches, the flow and heat transport in the pipe network are not considered. In a real GSHP system, the inflow and outflow temperatures on each individual BHE are time-dependent and closely coupled with the pipeline network. On the one hand, the heat flux on each BHE is determined by the temperature difference between the surrounding soil and the circulating fluid. On the other hand, the pipe network distributes and collects the fluid towards and from each BHE. The network itself has an intrinsic feature of balancing thermal extraction rates among different BHEs. Without the explicit consideration of hydraulic and thermal balance in the pipe network, the above mentioned coupling effect cannot be accurately quantified.

As the large BHE array is fairly new to the market, the current industrial standards and guidelines have not yet fully recognised coupled pipe network effect. Most of the guidelines just specifies a minimal distance between BHEs to mitigate the thermal interference. For example, Switzerland requires a minimum distance of 5 m is between the BHEs (cf. Miglani et al. [32]). In United Kingdom the value is 7 m [33]. The German guideline increased this value from 5 m to 6 m in its 2015 updated version [34, 35]. And in China this distance is kept between 3 m to 6 m [36]. The 2015 version of the Germany guideline VDI4640 [35] partially recognised the varying heat extraction rates by introducing a penalty factor when the GSHP system contains less than five

BHEs. For systems larger than that or bearing a capacity higher than 30 kW, numerical or analytical modelling studies become a mandatory requirement. After reviewing the state-of-art of current modelling approaches, one key scientific question emerges with regard to the system behaviour of large BHE arrays: How does the thermal extraction rate on individual BHE change in response to the thermal imbalance, which may occur due to insufficient thermal recharge in the long-term operation?

This study intends to answer the above question by introducing a comprehensive numerical model, with the shallow subsurface, the multiple BHEs and the pipe network explicitly quantified in a single numerical modelling framework. Section 2 explains the mathematical background of this numerical model. Section 3 verifies the model by comparing its result against analytical solution and by checking its thermal balance. In section 4, a series of numerical experiments were designed to quantitatively investigate the amount of shifted thermal extraction rate in large BHE arrays. Interpretations and discussions were further given to reveal how the three compartments, i.e. the subsurface, the BHEs, and the pipe network, are interacting with each other in response to supply heat or cool to the building. Additionally, the subsurface soil temperature distribution computed by the super-positioned infinite line source model were compared against the numerical model extended in this work, to see how much deviation it will be by assuming an imposed heat extraction rate on each BHE (section 6.1). This manuscript finalises itself with specific suggestions to the design of large BHE arrays.

2. Method

In this section, the theoretical background and the mathematical framework are presented.

2.1. Subsurface BHE model

The BHE used in this paper contains a single U-shape pipe (1U type). The details about its finite element realisation has already been described in Diersch et al. [37]. The cylindrical borehole is equipped with a 1U pipe and filled with grout. In the heating season the refrigerant with a relative low temperature is pumped into the BHE inlet (denoted with $i1$). It is circulated through the 1U pipe and exits the BHE at the outlet (denoted with $o1$). Due to the temperature difference between the fluid, the grout and the surrounding soil, heat flux is established and transfers heat into the pipe and rises the temperature of the circulating fluid. The fluid then goes through the pipe network and its carrying heat is supplied to the heat pump. The heat was transferred through three different media, namely the soil, the grout, and the circulating fluid. Following Diersch et al. [37] the governing equations for the heat transport between soil and grout reads

$$\frac{\partial}{\partial t}\left\{\left[\varepsilon\rho^f c^f + (1-\varepsilon)\rho^s c^s\right] T_s\right\} + \nabla\cdot\left(\rho^f c^f \mathbf{v} T_s\right) - \nabla\cdot(\Lambda\cdot\nabla T_s) = H_s. \quad (1)$$

In grout zone #1 (g1, same in zone #2),

$$\begin{aligned} &\frac{\partial}{\partial t}\left(\varepsilon_g\rho^g c^g T_{g1}\right) - \nabla\cdot\left(\varepsilon_g\lambda^g\nabla T_{g1}\right) = H_{g1} \quad in\ \Omega_{g1} \\ &with \\ &q_{nT_{g1}} = -\Phi^{1U}_{gs}(T_s - T_{g1}) - \Phi^{1U}_{fig}(T_i - T_{g1}) - \Phi^{1U}_{gg}(T_{g2} - T_{g1}) \quad in\ \Gamma_{g1}. \end{aligned} \quad (2)$$

For fluid within the pipe (e.g. the inlet side),

$$\begin{aligned} &\frac{\partial}{\partial t}\left(\rho^r c^r T_{i1}\right) + \nabla\cdot\left(\rho^r c^r \mathbf{u} T_{i1}\right) - \nabla\cdot\left(\Lambda^r\cdot\nabla T_{i1}\right) = H_{i1} \quad in\ \Omega_{i1} \\ &with \\ &q_{nT_{i1}} = -\Phi^{1U}_{fig}(T_{g1} - T_{i1}) \quad in\ \Gamma_{i1}, \end{aligned} \quad (3)$$

where, ε is the porosity, Λ denotes the thermal dispersion, H denotes the heat sink and source term. For hydraulic parameters $\mathbf{u}$ denotes the velocity of circulating fluid inside the pipe, and $\mathbf{v}$ denotes the Darcy velocity of ground water flow. The governing equations (1) to (3) can be simulated by the open-source scientific modelling software OpenGeoSys. The BHE feature in the OpenGeoSys has been verified against analytical and lab measurement data [30]. It has also been utilised to investigate the amount of extractable energy with both shallow [21] and deep borehole heate exchangers [31].

2.2. Pipeline network model

In order to investigate the effect of different pipe network layouts on the heat extraction rate of individual BHE in the array, the numerical model OpenGeoSys is coupled with the steady state power plant simulation software TESPy developed by Witte [38]. The TESPy software is capable of simulating coupled thermal-hydraulic status of the network, which is composed of pre-defined components including pipes, heat exchangers and different types of turbomachinery. In TESPy, governing equations were constructed to achieve steady-state mass and pressure balances for all connected components. On the mass balance side, the total amount of fluid entering into ($\dot{m}_{in,j}$) or flowing out ($\dot{m}_{out,i}$) of a component must be equal,

$$\sum_j \dot{m}_{in,j} = \sum_i \dot{m}_{out,i}. \tag{4}$$

On the pressure side, the pressure drop in a specific pipe can be calculated by the Darcy-Weisbach equation (Eq. (5), Böswirth and Bschorer [39]). As flow velocity is not part of the variables in TESPy, the equation implemented in TESPy is deduced by calculating flow velocity v through the pipes dimensions, the fluids density and mass flow rate. The Reynolds number Re is a function of pressure, enthalpy and flow rate. The fluids density ρ depends on pressure and enthalpy,

$$\begin{aligned} p_{in} - p_{out} =& \frac{\rho}{2} \cdot v^2 \cdot \frac{\lambda\left(Re, k_s, D\right) \cdot L}{D}. \\ =& \frac{8 \cdot \dot{m}_{in}^2 \cdot L \cdot \lambda\left(Re, k_s, D\right)}{\rho \cdot \pi^2 \cdot D^5}. \end{aligned} \tag{5}$$

Furthermore, energy balance (Eq. (6)) was imposed with respect to enthalpy for every component. The power P or heat transfer $\dot{Q}$ can be zero in certain cases where an adiabatic component does not transfer heat or a pipe does not transfer power,

$$\dot{Q} + P = \sum_i \dot{m}_{out,i} \cdot h_{out,i} - \sum_j \dot{m}_{in,j} \cdot h_{in,j}. \tag{6}$$

From Eq. (4) to (6), the coupled governing equations are highly nonlinear. For example, temperature changes of circulation fluid due to BHE operation will lead to the change of fluid density and viscosity, and they will further determine the pressure drop due to friction. To handle this, TESPy accesses the CoolProp library (Bell et al. [40]) internally for the fluid property calculation.

The component based architecture of the software allows the creation of individual model by connecting the respective components to form a topological network. By doing so, the characteristics of a specific pipeline network are defined by its own topology as well as the parametrization of the network's components. With these input information available, TESPy will automatically generate a set of nonlinear equations. The multi-dimensional Newton-Raphson algorithm is then adopted to solve the coupled equations for the primary variables mass flow, fluid enthalpy, and pressure at every point of the network as these variables fully determine the state of the circulating fluid. Thus, the total number of primary variables is equal to three times the number of connections between the network's components. After specifying the thermal load of the building, no matter how complex the network is, TESPy will be able to simulate the steady state temperature, pressure and mass flow rate throughout the pipe network. Interested readers may refer to the online documentation of TESPy for the details of corresponding benchmarks and tutorials [38].

2.3. Coupling OpenGeoSys and TESPy

According to Eq. (2) and Eq. (3), the thermal load of each BHE in a BHEs array is dependent on the soil temperature T_s around the BHE and the inflow fluid temperature T_{i1}, which is directly determined by the configuration of the pipeline network. Therefore, to obtain the thermal load on each BHE in the model, the soil temperature distribution and the hydro-thermal interference in the network should be simulated. In this study, the numerical model OpenGeoSys (OGS) [41] has been coupled with the Thermal Engineering Systems in Python (TESPy) [38] to explicitly simulate both the BHE and pipe network. The coupling was achieved through a Python interface. The schematised procedure of the method is illustrated in Fig. 1. Within every time step and each iteration, the outflow temperature T_{out} from each BHE is simulated by OGS and transferred to TESPy via the interface. The T_{out} and the current hydraulic state are then used as the boundary condition for the pipeline network simulation in TESPy. TESPy will calculate the current inflow temperature T_{in} of each BHE and their flow rate, which satisfies the overall thermal load of the building. These computed data will be transferred back to OGS for the next iteration. The convergence was achieved when the difference from the last two iteration results is smaller than a preset tolerance of 1×10^{-6}.

To be noticed is that the heat flow in OGS model is transient but the fluid and heat flow in the pipe network is steady state, therefore the model should not be applied for the short-term (minutes to hours) scenario simulations. In this study, our intention is to investigate the long-term behaviour of the

GSHP system, especially its response to over-exploration over a long time span. For this purpose, the time step size in our simulation was set to 3 hour (10800 seconds). With this time step size, the steady-state flow and heat transfer in the pipe network are well preserved.

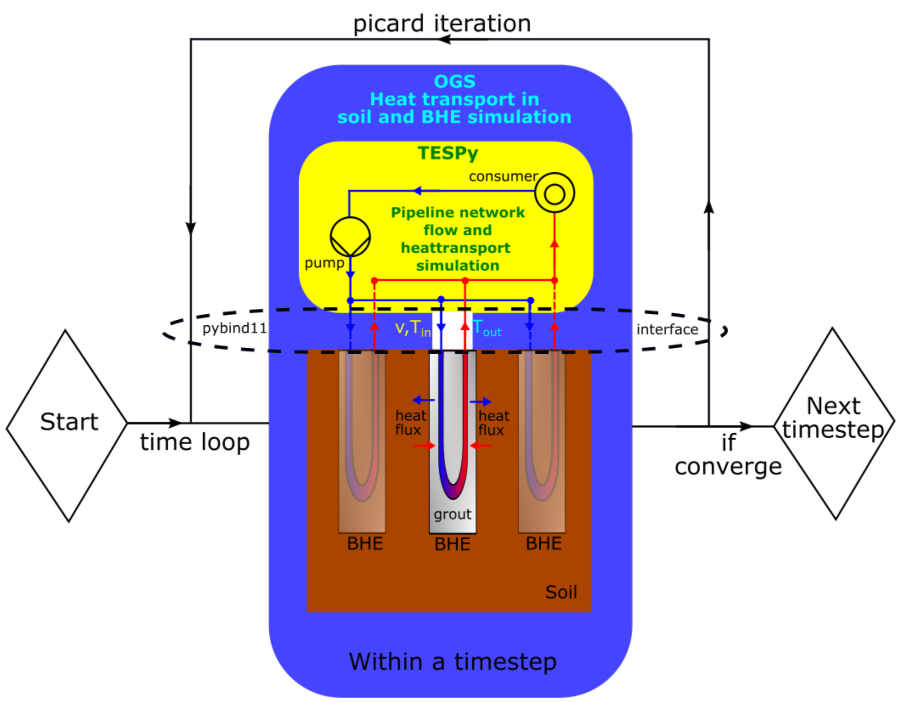

Figure 1: Coupling scheme of the TESPy (yellow) and OpenGeoSys (braun) software, the former simulates hydro-thermal processes in the pipe network and the latter models the subsurface heat transport around BHEs

3. Model verification

As there is no analytical solution to our knowledge that is capable of predicting the temperatures in subsurface and in the pipe network simultaneously, the multi-BHE array model developed in this work will be verified in two separate steps. For the subsurface part, the simulated soil temperature evolution by OpenGeoSys was compared with the super-position analytical solution. For the pipe network part, the system thermal balance was examined to ensure the correctness of the model implementation.

3.1. Verification of the multi-BHE array model

For verification purpose, a 2D numerical model containing 25 BHEs was set up. The model domain has a geometry of 300 × 300 m. The peripheries of the domain were no-flux boundaries. The location of 25 BHEs is shown in Fig. 2. They are organised in a 5×5 array with a constant distance of 6 m from each other. On each of these BHEs, a heat sink term was imposed, which is equivalent to the infinite line source in the analytical solution by Eskilson [8]. A sequence of heat extraction rate is imposed identically on each BHE. This sequence is following the load curve applied in section 4.2 and depicted in Fig. 7. Accounting a total length of BHE with 50 m, this translates to a specific heat extraction rate from a minimum of 0 W/m in the recovery months (May to August), up to 12.5 W/m in the peak month (January). A total of 10 years of BHE operation was simulated. For this setup, there exists the super-position analytical solution from Bayer et al. [15], which is capable of calculating the temporal temperature change at an arbitrary location (i, j). The mathematical formulation of Bayer's analytical solution reads

$$\Delta T_{i,j}\left(x,y,t,q_{k=1,\dots,n,l=1,\dots,m}\right)=\sum_{l=1}^{m}\sum_{k=1}^{n}\frac{q_{k,l}}{4\pi\lambda}\left(E_1\left[\frac{(i-x_k)^2+(j-y_k)^2}{4\alpha\left(t_m-t_{l-1}\right)}\right]-E_1\left[\frac{(i-x_k)^2+(j-y_k)^2}{4\alpha\left(t_m-t_l\right)}\right]\right), \tag{7}$$

where $q_{k,l}$ is a sequence of heat extraction pulses on the k_{th} heat source term at t = l time step. (x_k, y_k) denotes the location of the k_{th} BHE. E_1 refers to the exponential integral function. λ is the thermal conductivity and α is the thermal diffusion coefficient.

For the verification, simulated soil temperature was compared along the observation profile ($A - A'$) as shown in Fig. 2. It is selected to be 0.05 m away from the diagonal of the domain. The reason of keeping this distance is to avoid the exact location of each sink term, where the analytical solution will produce an infinite value. The Fig. 2a depicts the numerical and analytical results along the observation profile after 10 years of operation, and Fig. 2b illustrates the evolution of numerical and analytical results at the nodes located 0.05 m aside from the selected BHEs over the 10 years. The long-term extraction of shallow geothermal resources causes a temperature draw-down especially in the middle section of the BHE array. The numerical results fits visually very well with the analytical solutions. To give a more quantitative measure of the deviation, the error ϵ was calculated according to the following equation,

$$\epsilon = \frac{||T_{j,t} - \hat{T}_{j,t}||_2}{N_{dof}}, \tag{8}$$

where N_{dof} denotes the number of degrees of freedom (600 in Fig. 2a case and 120 in the Fig. 2b), $T_{j,t}$ and $\hat{T}_{j,t}$ are the analytical and numerical solution of the soil temperature at the t timestep and at the j_{th} node on the observation profile respectively. A relative small value of $\epsilon = 1.3 \times 10^{-4}$ and 1.6×10^{-4} was achieved for the two figures respectively, which proofed that the soil temperature distribution was correctly calculated by the numerical model OpenGeoSys.

3.2. Verification of the pipeline network model in TESPy

To verify the heat transport feature predicted by TESPy in the pipe network, a 25-BHE pipe network has been set up. The topological structure of the BHE system is illustrated in Fig. 6(c). All 25 BHEs are connected with each other in a double-layer parallel manner. The arrows in the figure indicates flow direction of the circulating fluid. Within the network, a pump was included to lift the hydraulic head and drive the fluid flow. The hydraulic balance within the entire network was verified against the results from the widely recognised software EPANET [42], which is the standard solution for the modelling of drinking water supply systems. The verification was completed by comparing the hydraulic head values at the connection points of the pipes. The EPANET and TESPy simulated results are nearly identical. The standard deviation of the results from two software is only 2.18×10^{-5} and

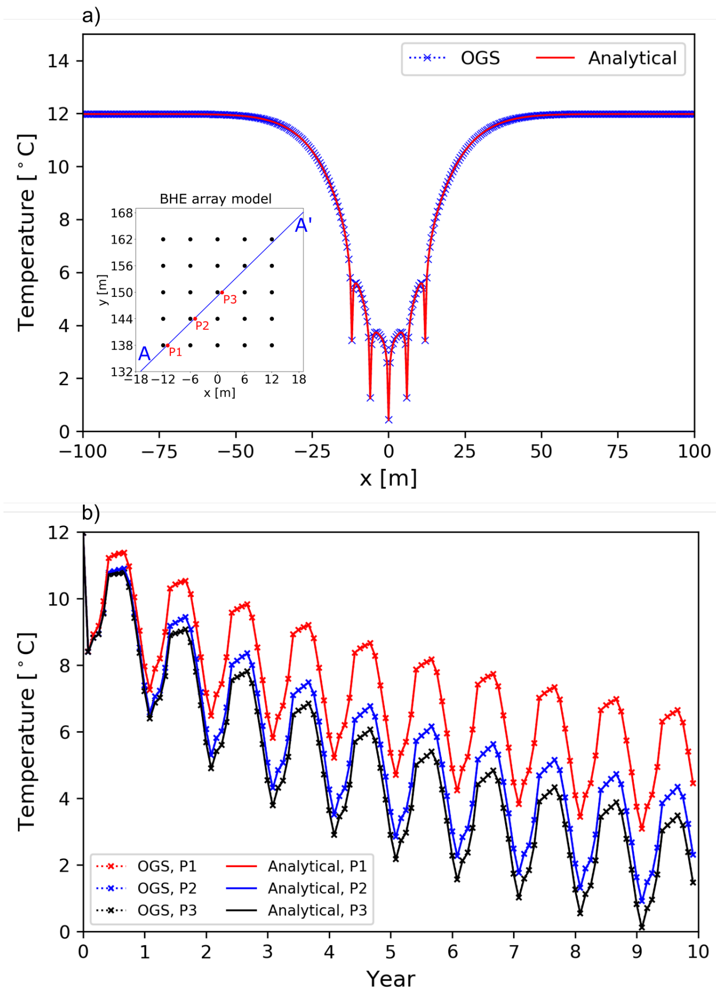

Figure 2: (a) Numerically simulated and analytically calculated soil temperature distribution along the observation profile (A-A') after 10 years of BHE operation; (b) Comparison of numerical and analytical result at locations 0.05 m aside from the BHEs over a 10-year-period.

the computed difference is mainly due to the different convergence conditions in each software. Due to limited space in this manuscript, details of the hydraulic verification is not included here. Instead, we will focus on the thermal balance of the system. Detailed description of the fluid circulating process within the entire pipeline system could be found in section 4.1.2.

In this case, a total of 10 years of BHE operation was simulated under different monthly heat demand strategy. An annual thermal demand curve was imposed on the heat pump, with the assumption that its thermal demand was supplied by the inter-connected 25 BHEs. The average heat extraction rate on each BHE differs over the months, but it can be obtained by normalising the total thermal demand over the number of BHEs (25 in this case). This calculated average heat extraction rate was illustrated as the black curve in Fig. 7. In each year the average heat extraction rate on each BHE varies from its peak (625 W) in January down to the minimum load (78.125 W) in September. From May to August the load is set to zero, which is the recovery period. Based on the mathematical framework described in section 2.2, the temperature and pressure distribution within the network could be computed by TESPy in each time step. Based on the temperature difference at the inlet and outlet of each BHE and the flow rate $\dot{m}$ within each pipe, OGS calculates the actual heat extraction rate on each BHE $\dot{Q}$ according to

$$\dot{Q} = (\rho c)_f \dot{m}(T_{i1} - T_{o1}), \tag{9}$$

where $(\rho c)_f$ is the circulating fluid heat capacity.

Form the results presented in Fig. 3, it can be observed that the heat extraction rate are unequal in different BHEs and they deviate from the calculated average value. This suggests that the thermal interference may already result in the shifting of extraction rate. In Fig. 3, the location of BHEs is marked with the index number as shown in Fig. 5. The six vertical columns with multiple colour dots indicate the varying total thermal load in different months. The simulated results showed that for BHEs at the centre of the array, it generally has an actual extraction rate lower than the average (below the black line). In the contrary, the BHEs at the outer part is sharing a higher thermal load (higher than black line). Considering the existence of thermal interference, it is physically reasonable that the actual heat extraction rates were deviating from the average value, but when looking into its annual trend, individual extraction rates are still largely controlled by the total system load. Since it is assumed that all supplied building heat comes from the BHEs, a virtual heat pump was added in the model, which does not consume any electricity or delivers additional heat to the building. Although the thermal load is not equally distributed, the total thermal load of the system should then be equal to the summation of actual heat extraction rates from all BHEs. We use this balance relationship to exam the correctness of the coupled model. Here the computed BHE heat extraction rate (after Eq. (9)) on each BHE were added up and the total value was compared against the imposed total thermal load (see Fig. 4). As shown in the Fig. 4, the comparison was nearly perfect with a R-squared value of 99.89%. The deviation attributes to the fact that the fluid density and viscosity were all assumed to be a constant in the OpenGeoSys code, while they were dynamically adjusted on the TESPy side. Despite of this negligible difference, the comparison gives us strong confidence that the coupling of heat transport between the OpenGeoSys and TESPy was correctly implemented.

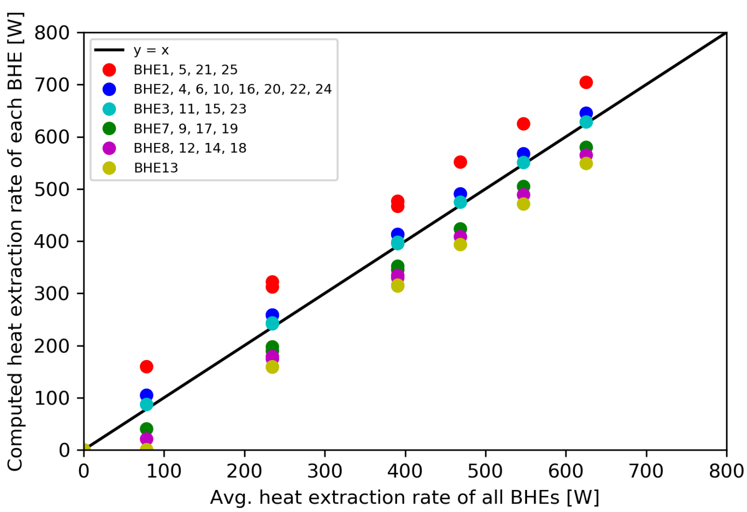

Figure 3: Regression plot of the actual computed heat extraction rate on each BHE against the average heat extraction rate of all BHE in different heating months in the 10_{th} year

4. Numerical experiments

In order to systematically investigate the shifting heat extraction rate as shown in the above section, three different BHE arrays were configured and

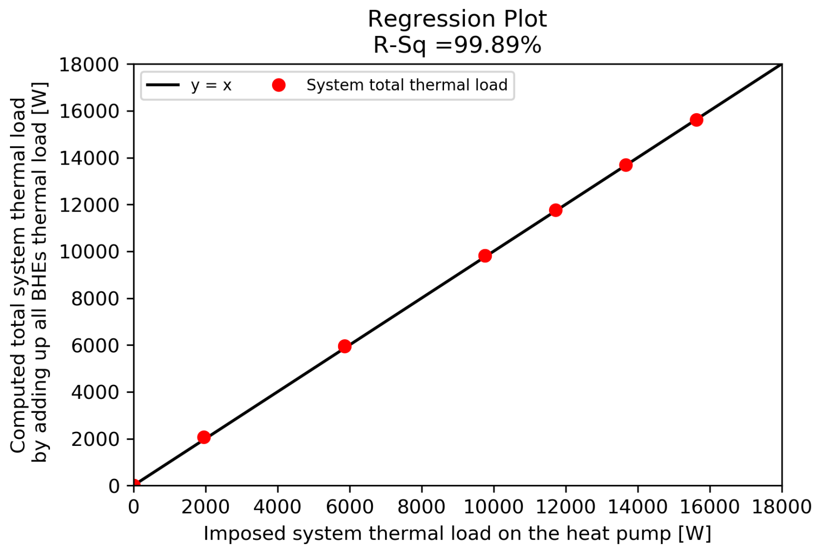

Figure 4: Regression plot of the computed heat extraction rate on all BHE against the imposed thermal loading at the heat pump in different thermal loading months over the 10_{th} year

simulated. Fig. 5 illustrates the domain representing the subsurface part, as well as the arrangements of the pipe networks. Fig. 6 further reveals how the pipes are connected in the three setups, namely the single BHE, the 3×3, and the 5×5 cases. The detailed configuration of each model with their parameter and boundary condition settings are described subsequently.

4.1. Model domain

4.1.1. Subsurface part

For the subsurface domain, a 300× 300 × 160 m mesh was constructed with prism and line elements. The total number of nodes and elements in the single BHE case was 3144 and 5530. For the 3×3 and 5×5 cases the numbers are 37248 and 68432 nodes, along with 70884 and 126197 elements respectively. The BHE arrays were installed always in the centre of the domain and composed of line elements in all scenarios. All BHEs have an identical length of 50 m, with its top located at a depth of 2 m. To satisfy the design requirement by the Germany VDI guideline [35], the distance between the adjacent BHEs is kept at a minimum of 6 m. Detailed parameters for soil, BHEs and circulating fluid applied in the model are listed in the Table 1.

Table 1: Parameters of the Soil, the BHE, the circulating fluid and the pipeline network adopted in the model

Parameter	Symbol	Value	Unit
Soil thermal conductivity	λ_s	2.4	$Wm^{-1}K^{-1}$
soil density	ρ_s	1120	kg/m^3
Soil specific heat capacity	$(\rho c)_s$	2.0×10^6	$Jm^{-3}K^{-1}$
Initial subsurface temperature	T_0	11.167	$^\circ C$
Length of the BHE	L	50	m
Diameter of the BHE	D	0.13	m
Diameter of the pipe in BHE	d_0	0.013665	m
Wall thickness of pipe	b_0	0.003035	m
Wall thermal conductivity	λ_0	0.39	$Wm^{-1}K^{-1}$
Grout thermal conductivity	λ_g	0.806	$Wm^{-1}K^{-1}$
Grout heat capacity	$(\rho c)_g$	3.8×10^6	$Jm^{-3}K^{-1}$
Circulating fluid density	ρ_f	992.92	kg/m^3
Circulating fluid thermal conductivity	λ_f	0.62863	$Wm^{-1}K^{-1}$
Circulating fluid heat capacity	$(\rho c)_f$	4.16×10^6	$Jm^{-3}K^{-1}$
Circulating fluid viscosity	η	0.00067418	$kgm^{-1}s^{-1}$
Circulating fluid flow rate	$\mathbf{u}$	0.00027	m^3/s
Length of the pipe for BHE in network	l	100	m
Diameter of the pipe for BHE in network	d	0.013665	m
Roughness coefficient of the pipe	k_s	0.0001	m

It is well known that groundwater flow, by bringing in additional recharge to the subsurface, will enhance the heat extraction capacity of the BHE array. The OpenGeoSys code used for the numerical experiments is also capable of simulating the system operation along with the groundwater flow process (see e.g. Hein et al. [21]). However, groundwater flow regime is strongly location dependent, and it may not be present in every geothermal site. As a result, an assumption of no groundwater flow was applied for all modelling scenarios

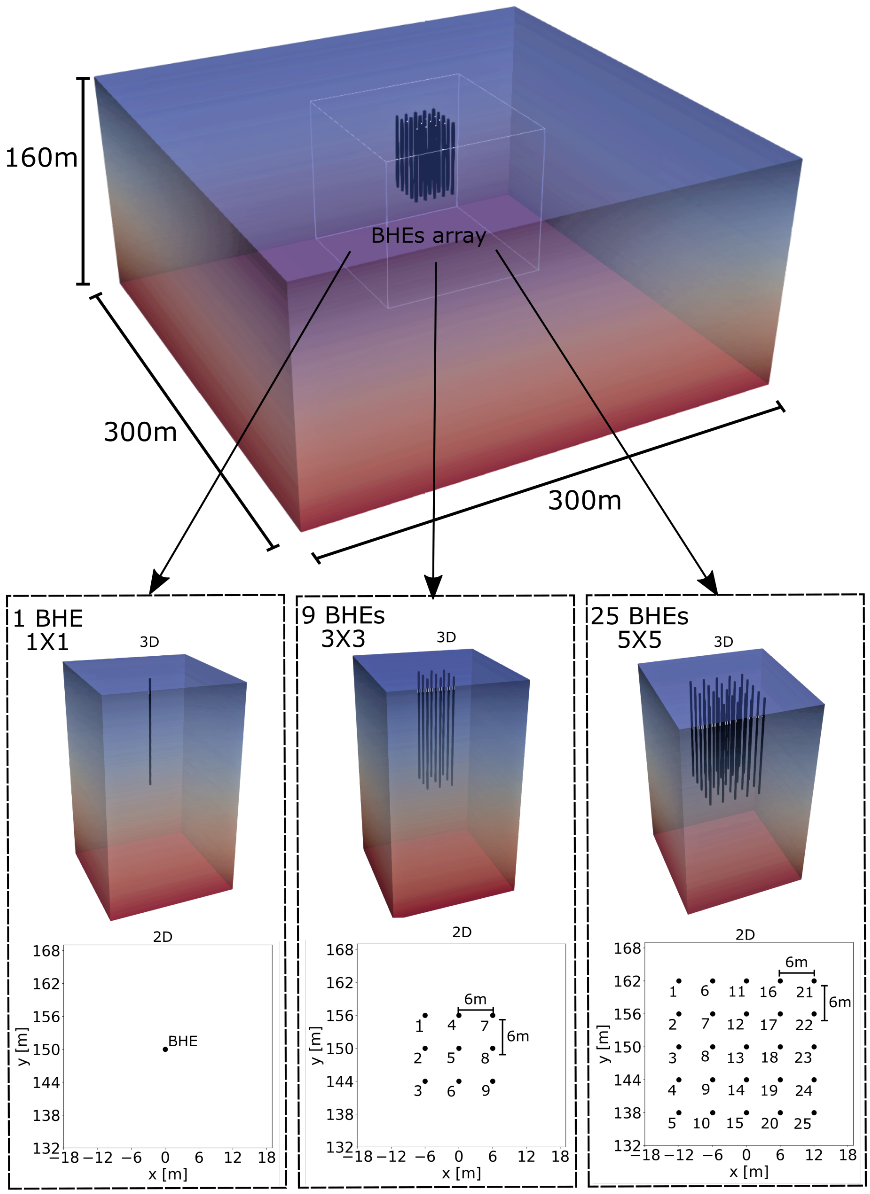

Figure 5: Location of the BHEs in the subsurface model (3D views and horizontal cross-sections)

in this study. This allow us to focus on the impact of thermal interference between BHEs.

4.1.2. Pipe network

A closed-loop pipeline network system was constructed in TESPy to couple with the OpenGeoSys model. Fig. 6(a) illustrates the basic configuration of the entire network with the single BHE case. After lifted by the pump, the circulating fluid will be divided into different branches by the splitter and then flow into each BHEs sub-arrays according to the pre-defined arrangement (see Fig. 6). In the 3×3 case, the system is divided into 3 sub-arrays, each of which are connected with 3 BHEs in a parallel way. In the TESPy setup, both serial and parallel connections can be constructed. The pure parallel scheme was chosen in this work for two reasons. Firstly the parallel connection is most applied in a realistic projects. Secondly, identical inflow temperature can be guaranteed on all BHEs in the array during the simulation. In the 5×5 case, the number of sub-arrays and the connected BHEs are increased. The fluid leaving the BHE will firstly be mixed at the merging point and then being extracted for heat extraction through the heat pump. The length and the diameter of the BHE pipe in the TESPy network are specified with the identical values as the properties used in the OGS model (see Table 1). Although the TESPy program is capable of simulating both the hydraulic and heat loss in the connecting pipes and the BHE, we have configured the model in a way that the hydraulic and heat loss along the connecting pipes are neglected. The reason behind this decision is to confine the heat loss only in the subsurface part and makes the thermal balance calculation in section 3.2 possible. Only with such simplification, the super-imposed line source model is equivalent to the numerical one in reproducing the subsurface temperature distribution. If the hydraulic losses in the connecting pipes are added, an equal distribution of flow rates among the individual BHEs are no longer possible, as the lengths of connecting pipes on each BHE are clearly different.

4.2. Initial and boundary conditions

OpenGeoSys

Considering the existance of the geothermal gradient in the subsurface, the initial soil temperature in OpenGeoSys is specified with an increasing trend along the depth. In the region of Leipzig area, the geothermal gradient value $\left(\frac{\partial T}{\partial z}\right)_{geo}$ is known from the measurement to be 0.016 Km^{-1} (cf. Richter et al.

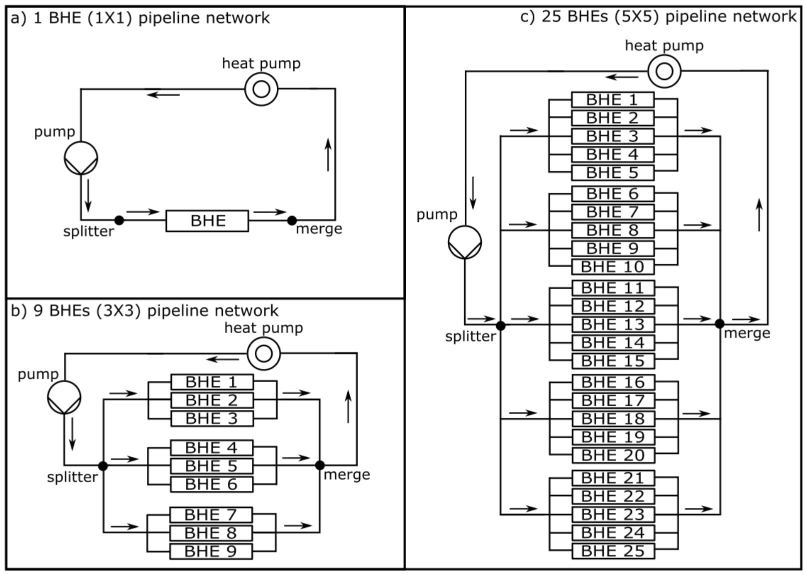

Figure 6: Arrangement of BHE pipeline network in TESPy

[43]). Starting from the surface, the initial soil temperature was set according to the average annual ground surface temperature of 11.167 °C, mimicking the Leipzig area. This value increases up to 13.727 °C at a depth of 160 m. As for the boundary conditions, an annual ground surface temperature curve is set, its variation is illustrated by the red line in Fig. 7. The temperature keeps constant within each month, its the lowest value is 2 $°C$ in December and January, then gradually increases to a maximum of 21 °C in June and July. A fixed geothermal flux with 0.0384 Wm^{-2} is imposed at the bottom surface as the Neumann boundary condition of the model. This value is based on the calculation of thermal flux $q_{geo} = \lambda_s \left(\frac{\partial T}{\partial z}\right)_{geo}$.

TESPy

In the three simulation scenarios, a fixed circulation flow rate with 0.27 kg/s was assumed within each BHE. Due to the parallel layout, the total flow rate through the circulation pump can be determined by multiplying the above flow rate with the number of BHEs in the array. Therefore, the total flow rate in the array was calculated to be 2.43 kg/s and 6.75 kg/s for the two larger arrays respectively. The Darcy-Weisbach equation (Eq. (5)) was adopted to quantify the pressure loss due to friction in the pipeline. As for the total thermal load in each modelling cases, a seasonal dependent curve was specified (cf. Fig. 7). Every year, a peak thermal load was found to be in January, with a specific heat extraction rate of 12.5 W per meter length of BHE. For the single BHE case, this translates to 625 W of thermal load. In the 3×3 and 5×5 cases, the total thermal loads were proportionally increased to 5625 and 15625 W. In other months, due to elevated environmental temperature, the thermal load was decreased. The general trend of this load curve was following Hein et al. [30]. It should be noted that the heat extracted from the BHEs serves as a heat supply of a heat pump. Thus, the actual heat supplied by a full system with a heat pump is much higher depending on the heat pump's COP. As the focus of this paper is on the BHE system instead of the heat pump, we choose this configuration in a way that the modelling result will not be influenced by the varying heat pump efficiency. Therefore, a virtual heat pump was added, by which all heat extracted from the subsurface will be transferred to the building side. No electricity was consumed by the heat pump. The advantages of this configuration is that the model can be verified with respect to its total thermal balance (as already shown in section 3.2) and the shifting thermal extraction rates inside the BHE array can be clearly demonstrated. In reality, this is definitely not the case. TESPy can also be programmed to simulate heat pumps with its COP depending on the fluid temperature. We will demonstrate this feature in future publications.

All three cases were simulated for a period of 10 years. The time step size was controlled to be 10800 seconds (3 hours). The simulation was carried out on a workstation equipped with 3.40 GHz CPU, 16 GB of memory. The model was configured to run in a serial mode without any parallelization scheme, i.e. only 1 CPU core was employed. The time needed for running the simulation depends strongly on the number of BHEs and the size of mesh correspondingly. For the single BHE case, the model simulation can be completed in 4.5 hours. In the 3x3 and 5x5 cases, this increases to 74 and 144 hours.

5. Results

In this section the simulated results from multiple scenarios defined in section 4 are presented. The thermal interference, and hence the shifted thermal extraction rates on individual BHEs are analysed accordingly. The three BHE arrays are composed of 1, 9 (3×3) and 25(5×5) BHEs. In each

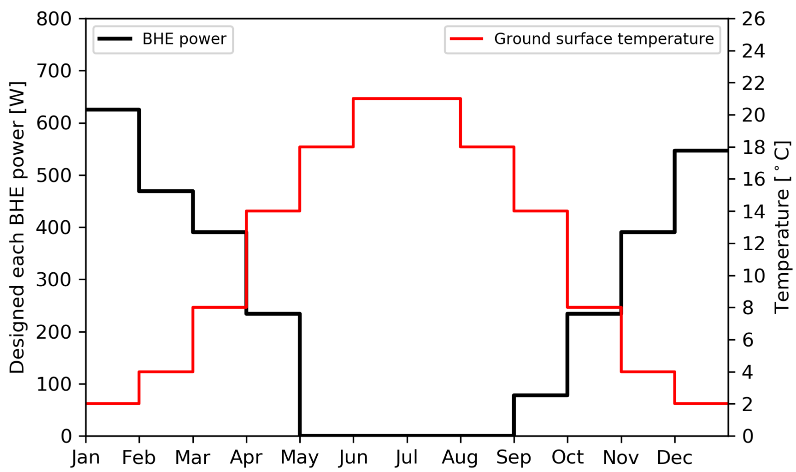

Figure 7: Annual ground surface temperature curve and seasonal average heat extraction rate on each BHE

of the setup, BHEs located on some representative locations are selected and analysed. They are numbered as the BHE #1, #4 and #5 in the 3×3 case, and the BHE #1, #6, #7, #11, #12, and the #13 in the 5×5 case (see Fig. 5 for details).

5.1. *Evolution of temperature*

Fig. 8 depicts the soil temperature distribution in the 5×5 setup after 10 years. The left figure illustrates the 3D view of the temperature distribution near the centre of the BHEs array. A horizontal profile $Z - Z'$ at the depth of 27 m was depicted on the right. It can be observed that there exists a low temperature zone in the centre of the BHE array, indicating a thermal imbalance in the subsurface. To show this in a more quantitative way, Fig. 9 depicts the simulated evolution of soil temperature at 1 m distance from the selected BHEs at the same depth in the end of January every year, when the system is imposed with the peak heating load of that year. For comparison, the result of 1×1 BHE is also illustrated in both figures as the reference (black line). It can be observed that the soil temperature decreases gradually over time, due to the thermal interference between neighbouring BHEs. For the single BHE, the temperature reduction is the minimum, only about 0.6 °C after 10 years. After around 3 years, the soil temperature is already approaching a quasi-steady-state. Compared to the single BHE case, the temperature decrease in the 3×3 setup is much stronger. The temperatures at three different locations dropped by at least 2.6 °C after 10 years. The most intensive temperature decrease is found in the 5×5 case, where a reduction of at least 4 °C can be observed. Since the average heat extraction rate (625 W) on the individual BHE is identical, the 5×5 case has the maximum total system power (15625 W). In both the 3×3 and 5×5 cases, the soil temperature at the edge (BHE #1 in the 3×3 and 5×5 case) is general higher than that in the centre part of the array. When moving from the edge towards the centre, the temperature decrease also becomes larger. Since the soil at the centre is suffered by the most intensive accumulative effects from all sides, the soil temperature drop there is the most significant.

Similar trends can be observed in the evolution of BHE inflow and outflow temperature in the end of January, when the system is imposed with the peak heating load of each year, as illustrated in Fig. 10. The inflow and outflow refrigerant temperature in the single BHE case decreases slightly during the beginning 2 years and then stabilises at 3.8 and 4.3 °C respectively. Compared to that, the temperature drop in the multi-BHE array cases is considerably larger. In the 3×3 case, the inflow temperature is about 1.5 °C and the outflow remains at about 2.1 °C after 10 years. In the 5×5 case which more BHEs are coupled, a much lower inflow and outflow temperature were observed, with a minimum temperature of -0.2 °C and 0.4 °C respectively. Similar to the change of soil temperature as presented above, although the specific heat extraction rate remains the same in all cases (12.5 W/m). The inflow refrigerant was forced to decrease to a lower temperature when a larger BHE array is present. This is because, the increase in the number of BHEs connected in the system is also linearly related to the total amount of thermal load imposed. The insufficient recharge of heat in the shallow subsurface can only be balanced with a decreasing temperature in the circulating refrigerant. As demonstrated in Fig. 9 and Fig. 10, the circulating temperature in the 3×3 and 5×5 cases are also different over time. It suggests that the ability of each BHE to extract heat from the subsurface is deteriorating once the extracted thermal energy is beyond the recharging capacity of the subsurface.

It needs to be noticed that although the soil, BHE inflow and outflow temperature is dropping over time, the inflow and outflow temperature on different BHEs in the same array are not deviating much away from each other at the same moment. For example, in 3×3, the maximal outflow temperature difference was observed between BHE #1 and BHE #5 with 0.06 °C after 10 years. Compared with it, the difference increases slightly up to value of 0.14 °C between BHE #1 and BHE #13 in in 5×5. The reason for the different evolution of the outflow temperature on each BHE within a mult-BHE array is due to the different soil distribution near each BHE in the array over the time, which is showed in the last Fig. 9. Since the inflow temperature of all BHEs in each array arrangement keep identical due to the system parallel connected network, it indicates the ability for heat extraction on each BHE is different from the other during the system operation.

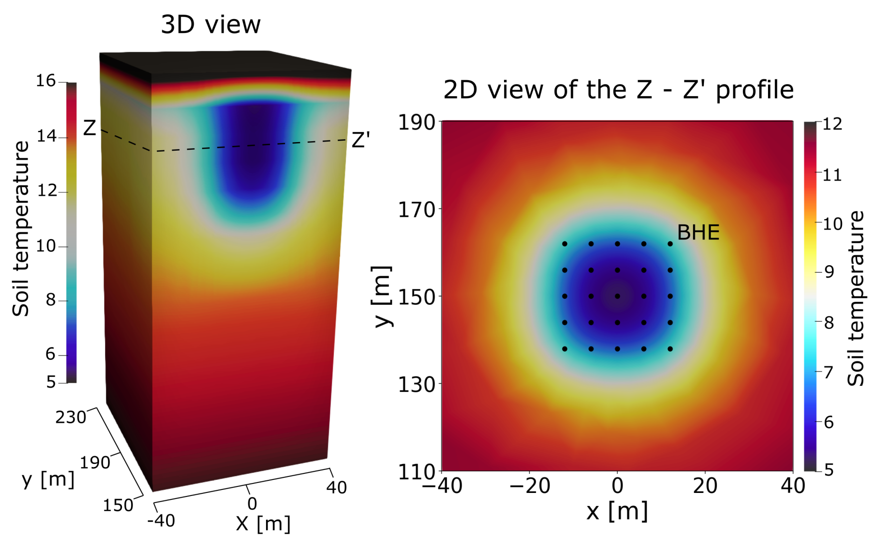

Figure 8: Distribution of soil temperature in 5×5 setup after 10 years, 3D view of one the left and horizontal profile at the depth of 27 m on the right

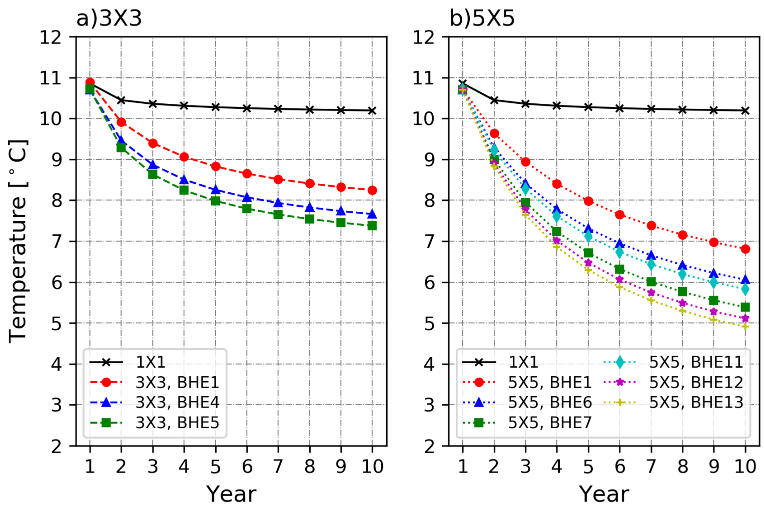

Figure 9: Evolution of soil temperature over 10 years at 1 m distance from the selected representative BHEs at a depth of 27 m in the end of January

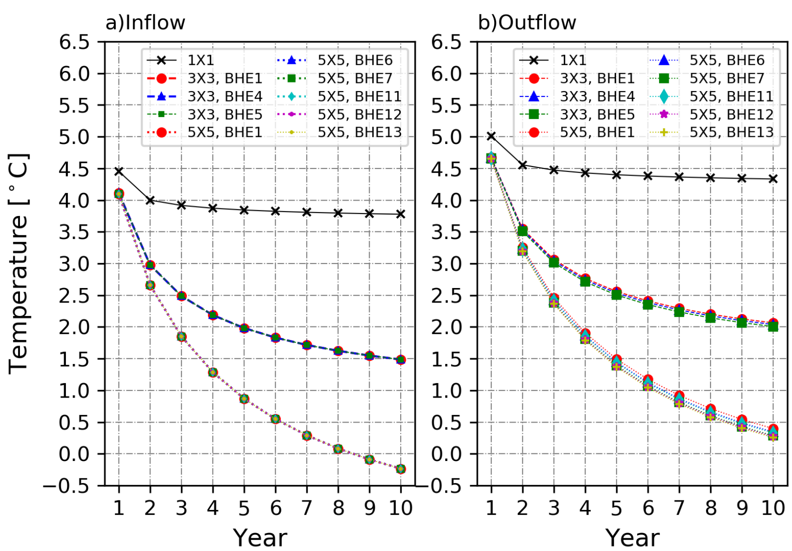

Figure 10: Evolution of BHE inflow (a) and outflow (b) temperature in the end of January (peak heating load) over 10 years with different array arrangements

5.2. Shifting of thermal extraction rates

With the available data in Fig. 10, the actual average thermal extraction rate on each individual BHE $\dot{Q}$ can be calculated with Eq. (9) and analysed for the 10-year-long simulated period. For each individual BHE, their actual individual heat extraction rate is compared to the system average value $\dot{Q}_{mean}$ (cf. Fig. 7). Followed by this logic, the simulated data can be further treated. First, the amount of shifted thermal load $\Delta\dot{Q}$ was calculated for each BHE by subtracting the heat extraction rate $\dot{Q}$ with the system average value $\dot{Q}_{mean}$. Then the shifted load is further normalised by the average value to show its proportion. The proportion of the shifted thermal load a is defined with the following Equation,

$$a = \Delta\dot{Q}/\dot{Q}_{mean}. \tag{10}$$

Firstly, the evolution of amount of shifted heat extraction rate $\Delta\dot{Q}$ was investigated. The Evolution of this "shifted load" is illustrated in Fig. 11. A few interesting phenomenon can be observed:

- In both array setups, the performance of the heat extraction rate on each BHE can be classified into two categories: BHEs located at the outer part of the array are experiencing a heat extraction rate increase (e.g. BHE #1 in 3×3; BHE #1, BHE #6, BHE #11 in 5×5), while the BHEs located at the inner part of array are experiencing a value reduction (BHE #4, BHE #5 in 3×3; BHE #7, BHE #12, BHE #13 in 5×5). For BHEs located at the edge and in the centre of the array, the maximal increase and reduction evolution are observed respectively. It indicates that the thermal load was systematically shifted away from the centre towards the outer part of the array through the operation of the pipe network.

- In the 3×3 array, the maximum change of heat extraction rate of -48 W was observed in the BHE #5 located at the centre. Compared to it, the maximal value with 89 W was observed on BHE #1 at the edge in the 5×5 setup, which means the shifting effect is enhanced in the larger array setup.

- In the 3×3 setup, the shifted heat extraction rate changes intensively for all BHEs in the first 2 years, before a quasi-steady-state is reached. Whilst in the 5×5 case, reaching the quasi-steady-state will take more than 5 years. It indicates the system with a larger array setup needs more time to reach the balance.

- In the 3×3 case, the shifted heat extraction rate of all BHEs becomes smaller after the recovery period every year, For instance he shifted rate on BHE #5 located at the centre changes its value from -47 W to -30 W after the recovery period in the 10th year. In the 5×5 case, the change of shifted heat extraction due to the recovery becomes smaller compared to that in the 3×3 setup. The maximum shifted heat extraction rate due to recovery was observed on BHE #1 at the edge with only 6 W. The shifted rate on BHE #6 and BHE #13 becomes even larger after the recovery. This indicates the recovery of subsurface heat will mitigate the heat extraction rate shifting. Yet, its effect will gradually weaken with an increasing number of installed BHEs.

On the other hand, the shifting situation could be presented with respect to its proportion in comparison to the mean value (see Fig. 12). Over 10 years' period, the change of this proportion a follows the similar trend as the $\Delta\dot{Q}$ in Fig. 11. Apart from this similarity, two phenomena were noticed. Compared to the trend of $\Delta\dot{Q}$, the proportion a varies much more intensively within every year. Besides, in the 5×5 case, the maximum proportion value exceeded 100% after 9 years. This means the BHE located at the centre was experiencing a negative thermal load during the heating season. It suggests that partially closing those BHEs located in the array centre for a certain period will be helpful to increase the efficiency of the entire system. Also, as shown in Fig. 12, the range of shifted heat extraction rates are elevated from 3 to 40% in the 3×3 case up to 12 to 105% in the 5×5 case. It means a more intensive shifting can be expected with increasing number of installed BHEs. This behaviour was also reported by Gultekin et al. [44] in their analytical formulation. In addition, according to Guiltekin's research, the adjacent distance among the BHEs is also an important factor to affect the thermal interaction in the BHE array. In this work a distance of 6 m was assumed, which is the minimum value allowed by the German guideline. How the distance can be optimised to mitigate the shifting behaviour would be one of the critical issues for future investigation.

5.3. Seasonal and long-term behaviour

In Fig. 13, the shifted heat extraction rate of BHE was depicted over the 10th year, when the quasi-steady-state has been achieved. In both ar-

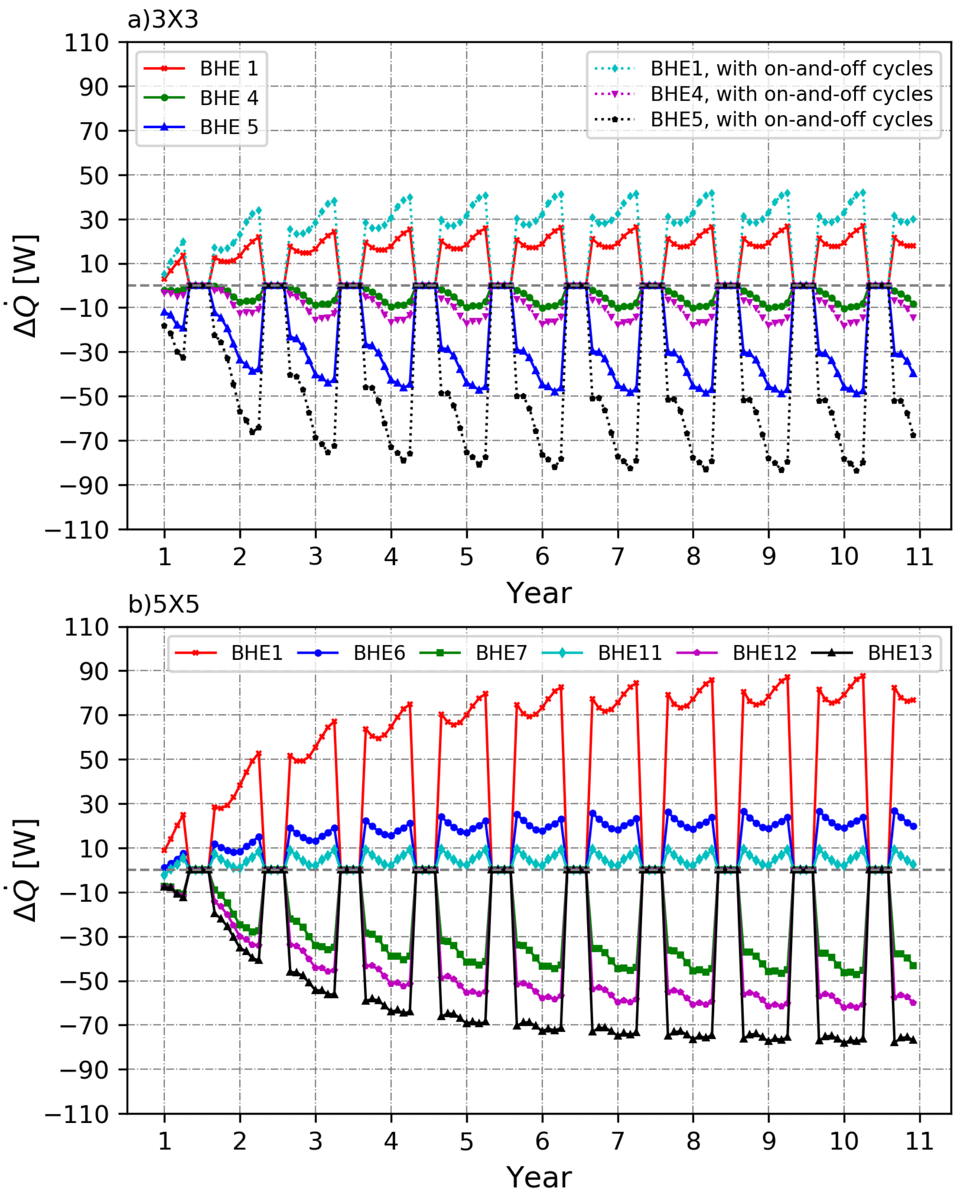

Figure 11: (a) Evolution of the shifted heat extraction rate of BHE in 3×3 over 10 years; (b) Evolution of the shifted heat extraction rate of BHE in 5×5 over 10 years.

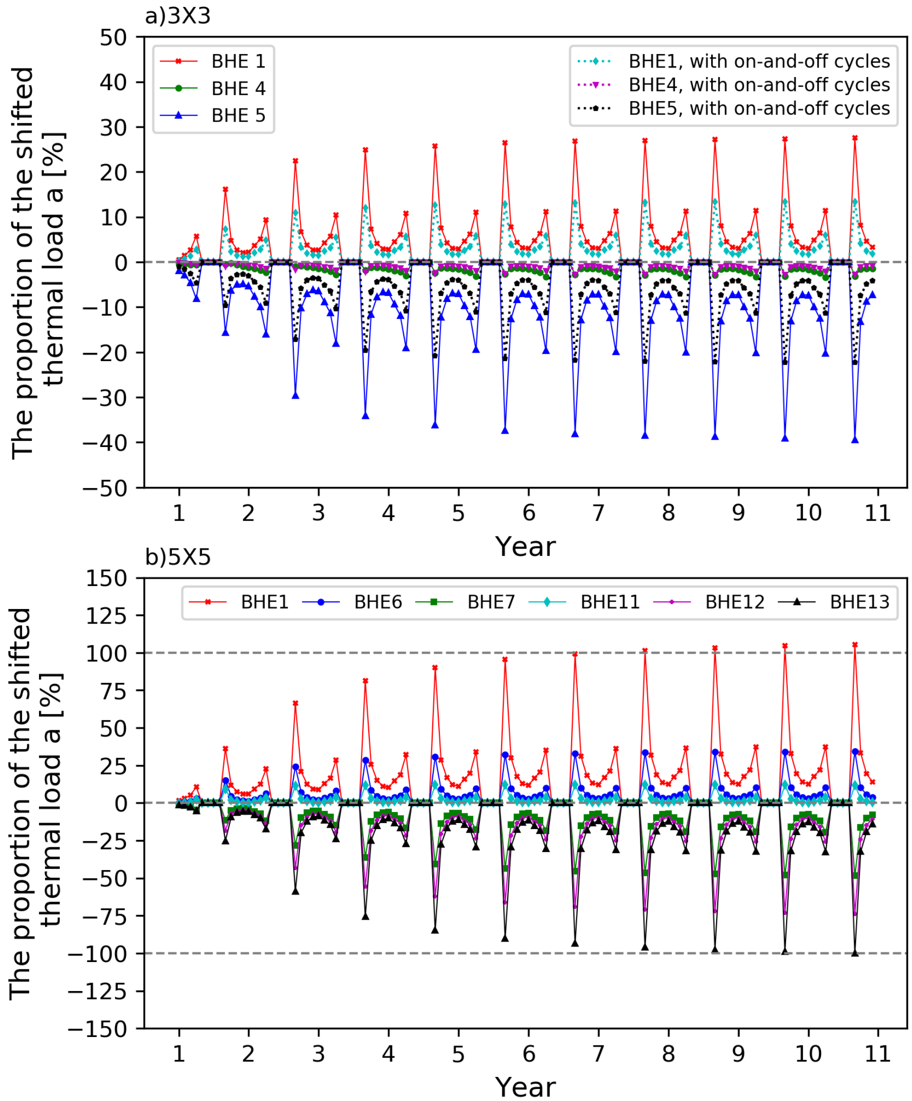

Figure 12: (a)Evolution of the shifted heat extraction rate proportion of BHE in 3×3 over 10 years;(b)Evolution of the shifted heat extraction rate proportion of BHE in 5×5 over 10 years.

rangements, with absolute amount of shifted thermal load $\Delta\dot{Q}$ change very slightly over the heating month (17 W maximum in the 3×3 case, and 11 W maximum in the 5×5 case). However, the picture is considerable different when the percentage of shift was calculated. The maximum percentage of shift a was observed to be 40% and 105% respectively in September, when the lowest heating demand was imposed. The minimum percentage of shift a is 3% and 12% in January, when the highest heating load was present. The result indicates the shifting behaviour has a minor impact on the system in the peak heating month, but it overall influence can be significant when the total thermal load is low. As shown in the section 5.2, the evolution of the shifting heat extraction rate is strongly time dependent. It is further analysed here with respect to its seasonal and long-term behaviour.

5.3.1. Long term behaviour

As shown in Fig. 11, the heat extraction rates on BHEs located inside the array were depressed over time in both arrangements, while the rates on those at the outer part were elevated gradually. The maximal reduced rate was observed on the BHE at the center, with -50 W in the 3×3 and -80 W in the 5×5 arrangement. The maximum elevated rate was on the BHEs located at the edge, with +27 (3×3) and +89 W (5×5). It becomes evident that over the long-term operation of the BHEs array, the heat extraction rate at the centre of the BHEs array is shifting gradually towards the periphery. Such shifting behaviour has also been confirmed in the study conducted by You et al. [28] through an analytical approach. Over the 10 years' long operation, the time necessary to achieve the quasi-steady-state depends heavily on the size of the BHE array. It requires 3 years to achieve a stable amount of shifted thermal load in the 3×3 case, while this time increases to 6 years in the 5×5 case. Typically, the system with a larger thermal demand requires a longer time to reach equilibrium with the thermal recharge in the subsurface.

5.3.2. Seasonal behaviour

Besides the long-term behaviour discussed above, the shifting also demonstrates different patterns within a single year over different seasons. In Fig. 13, the amount of shifted thermal extraction rates were plotted over the 10th year, where the quasi-steady-state of the system has already been reached. In both the 3×3 and 5×5 arrangements, the absolute amount of shifted heat extraction rate on each BHE remains quiet stable, although the total system thermal load changes intensively in each month. As a result, when the lowest total thermal load was imposed in September, the highest percentage of shifting was observed on BHEs located at the centre of the array. This phenomenon will enhance itself when the system size grows larger. For example in the 5×5 arrangements, a more than 100% reduction of the heat extraction rate was found on BHE #13 after 9 years of operation. At the same time, the heat extraction rate have been doubled on BHE #1, which is located at the edge. This suggests that BHE #13 is recharging the subsurface with the heat extracted from outer BHEs in this particular month, and the system load is solely supplied by those BHEs at the periphery of the field. It also suggests that the BHEs located at the outer part are more important to maintain the system working status during operation. It should be noticed that such seasonal behaviour is not unique and was also reported by other researchers in the literature. For example, Bayer et al. [15] observed similar pattern and developed an optimisation strategy based on it. They suggested that a given number of critical BHEs located at the centre should be disconnected from the array to improve system efficiency. With the newly extended numerical model, a more accurate prediction can be made on the inflow and outflow temperature on each BHE, with the recharge and thermal interference effect explicitly considered. Hence the design of optimisation strategy may also benefit from the numerical model from this work.

5.4. Heat extraction rate Shifting behavior with daily switch on and off cycles

In reality, a GSHP system may not work continuously all the time. Being aware of this fact, a scenario with daily on-and-off thermal load was simulated with the 3×3 BHEs configuration for a period of 10 years. The heat pump was assumed to be operating for 8 hours everyday, accompanied with a 16-hour long recovery period. To maintain a fair comparison, the same amount of heat has to be extracted from the subsurface. The thermal load on the BHE array was then tripled in comparison to other scenarios (see the curve in the Fig. 7). With this configuration, a 37.54 W/m specific heat extraction rate on each BHE was reached in the peak month (January) every year. In the modelling result, The soil temperatures at 1 m distance from the centre BHE #5 at a depth of 27 m dropped by 5.2 °C after 10 years, which indicating the existence of the underground soil thermal imbalance. The dotted lines in Fig. 11 and Fig. 12 depict the evolution of shifted heat extraction rate in the on-and-off scenario. The trend of shifting largely remains the same. It suggests that the daily recovery cycle has only limited impact. Besides, due to the tripled peak thermal load, the minimum inflow and outflow temperature

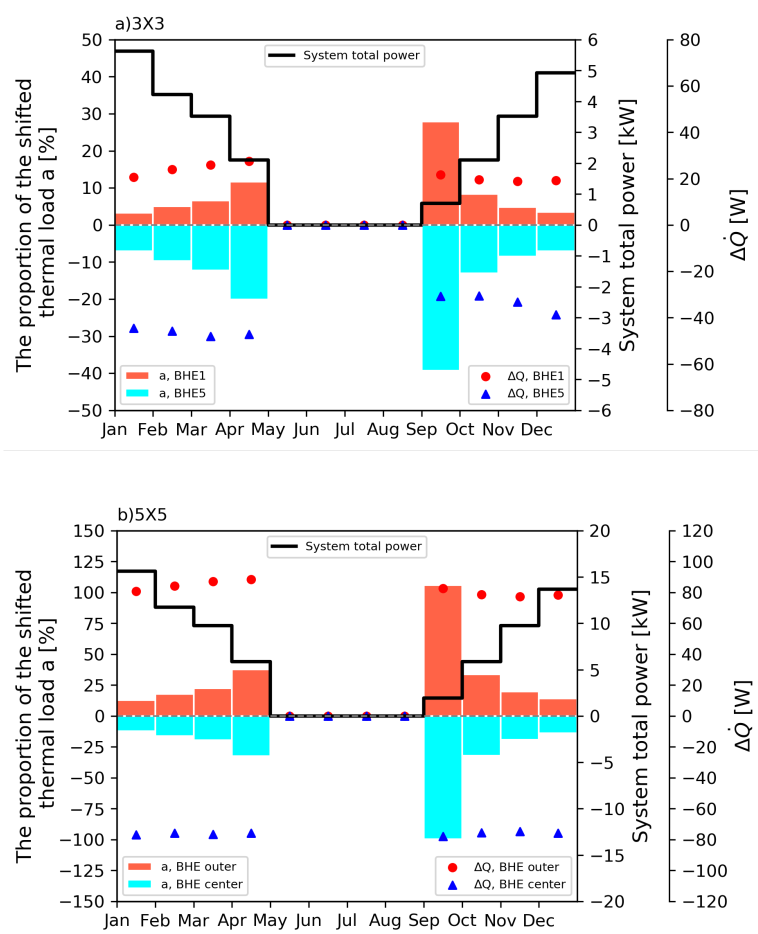

Figure 13: Seasonal behaviour of shifted heat extraction rate on individual BHEs over a single year with (a) 3×3 and (b) 5×5 arrangements in the 10th year

shows a much deeper draw-down in comparison to other scenarios. These values were found to be -8.5 °C and -6.8 °C respectively. This implies that the short-term (within the heating season) temperature evolution is more determined by the peak thermal load, while the long-term (over multiple years) development is largely controlled by the subsurface thermal recharge.

6. Discussion

6.1. Implication for super-position based analytical solution

As has been discussed in the introduction of this work, most super-positioned infinite line source models assume a constant heat extraction rate on each BHE and also do not consider the thermal interference as shown in this work. The soil temperature distribution computed by such approaches may lead to considerable deviation in comparison to the reality. It is thus meaningful to quantify such deviation by comparing results from the traditional analytical approach and the the newly extended numerical model. For this purpose three configurations were designed based on the 25 BHEs scenario as in section 4. The model was calculated for 10 years with 3 different configurations. In the first case, the super-position method as described in section 3 with Eq. (7) is applied to predict the soil temperature distribution. Then, OpenGeoSys numerical model was simulated both without (case 2) and with the pipe network (case 3). In case 2, each BHE was imposed with the same annual thermal extraction rate curve (black line illustrated in Fig. 7) over the heating season. In case 3, a total thermal load was calculated by summing up the heat extraction rate curves of each BHE and it was imposed on the pipe network. In this case, re-distribute of the total load is allowed among different BHE. The soil temperature distribution on the observation profile (A-A') was depicted at a depth of 27 m and compared in Fig. 14.

As shown in Fig. 14a, a clear deviation can be observed with respect to the soil temperature distribution predicted by the analytical and two numerical approaches. A maximum 2.5°C difference (cf. Fig. 14b) was obtained between the analytical against numerical result. The result from analytical approach consistently predicts lower soil temperatures. It confirms our hypothesis in the introduction that the seasonal ground surface temperature and bottom geothermal flux will contribute to the subsurface recharge (see also the results by Hein et al. [30]). It needs to be noticed that the peak seasonal average specific heat extraction rate on each BHE is assumed to be 12.5 W/m in this study, which is considerably lower than the usually applied load in field application (at around 20 to 35 W/m). It suggests that a larger deviation in soil temperature will be produced by the analytical approach. Compare to this effect, the soil temperature deviation caused by the shifted thermal load among BHEs is around ±0.3°C as demonstrated by the blue curve in Fig. 14b. This suggests the thermal interference and shifted thermal load does lead to a different soil temperature distribution. Yet, such deviation is rather negligible if compared to the one caused by the recharging effect.

The above comparison leads to several implications for the applicability of the analytical and numerical approaches. For long-term and high thermal load (e.g. thermal storage) applications, ignorance of the subsurface recharge process will over-estimate the draw-down in soil temperature. In such kind of applications, analytical results based on infinite line source model and super-position principle may lead to deviation in the soil temperature distribution. Hence, the application of such analytical approach should be limited. However, if the specific heat extraction rate is relatively low, as the value of 12.5 W/m case demonstrated in this study, the soil temperature deviation is very limited (<0.5°C) with or without considering the shifting of thermal load through pipelines.

6.2. Total thermal load on the BHE array

In recent years, there are increasing number of large BHE array systems installed in densely populated cities, with the intention to fully explore the potential of shallow geothermal resources. Bayer et al. [7] suggested in their work that the thermal interference between adjacent installations could be critical and affect the potential exploitation capacity of the system. As shown into our results in sections 5.1, Bayer's concern is validated, as the soil temperature and the circulating fluid temperature decrease intensively with the increase of the total thermal demand. In extreme cases, this may lead to freezing in the vicinity of the BHE or the failure of the heat pump [22, 45]. To avoid that, the German guideline VDI4640 [35] has imposed a lower limit of -5°C on the inflow temperature of each BHE. In this work, each BHE is set to have an identical length (50 m), and all the modelling scenarios were configured in a way that the average specific heat extraction rate on each BHE was configured with the same annual load curve (cf. Fig. 7). The total system load was increased in proportion to the number of BHEs connected

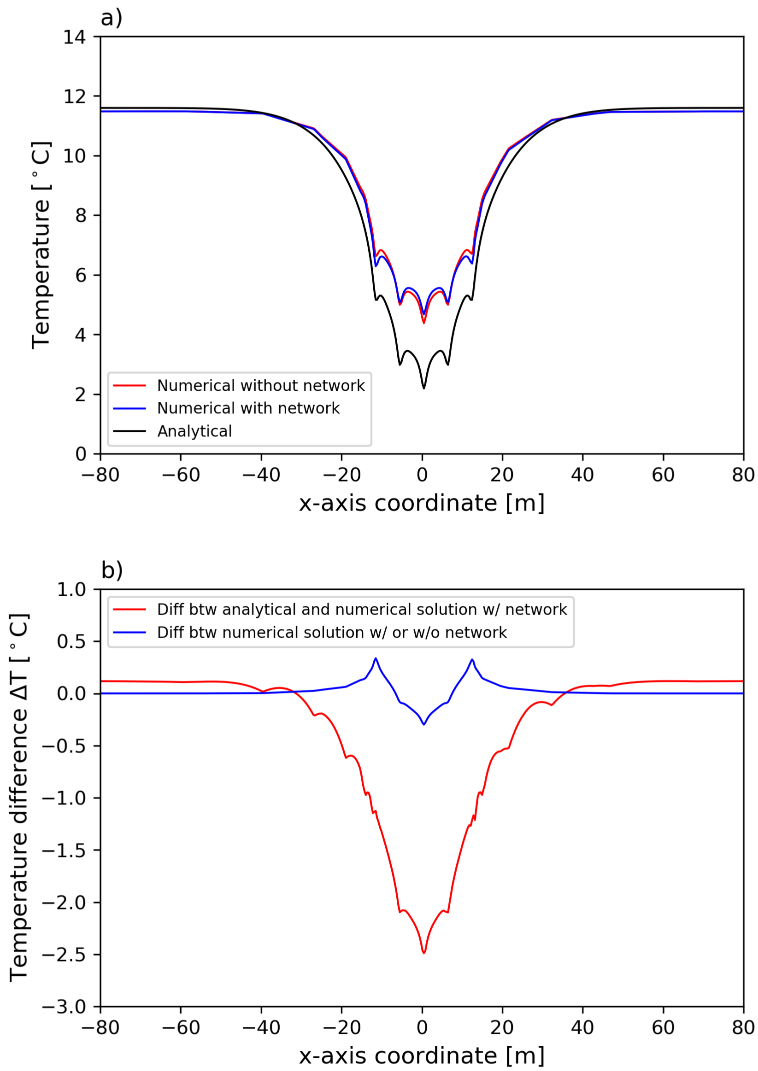

Figure 14: (a) Soil temperature distribution over the profile (A-A') at a depth of 27 m after 10 years of BHE operation, predicted by analytical and two numerical approaches with or without the pipe network (b) Red line: Analytical solution minus the numerical solution with network; Blue line: Numerical solution without network minus the one with network

in the array. In the simulated results, an important phenomenon that caught our attention is the decreasing inflow temperature along with the increasing size of BHE array, which can be viewed in the data listed in table 2 (an additional case with 7 × 7 BHEs were also added). Following the data, a minimal inflow temperature was at 4.4°C with a 12.5 W/m average specific heat extraction rate. When the size of array grows, the minimum value of inflow temperature in other scenarios decreases with the increasing number of BHEs. As the inflow temperature is constrained to be no less than -5°C according to the guideline, it suggests that the array size cannot be expanded arbitrarily.

Table 2: Minimal inflow temperature of BHE in the modelled scenarios after 10 years operation

BHE array	Number of BHEs in the array	Total BHE Length in [m]	System thermal load in [W]	Peak average specific heat extraction rate on each BHE in [W/m]	Minimal inflow temperature in [°C]
1 × 1	1	50	625	12.5	3.8
3 × 3	9	450	5625	12.5	1.5
	9	450	5625	37.54 (8-hour on and 16-hour off)	-8.5
5 × 5	25	1250	15625	12.5	-0.2
7 × 7	49	2450	30625	12.5	-1.5

Meanwhile, along with the increasing size of BHE array, its influencing size is also extended. For instance, in the last section 6.1 a temperature influence range in the soil part extends to about 40 m (cf. Fig. 14) after the long-term operation. This suggests that heat from the neighbouring subsurface has been exploited already. With this result in mind, the size of the array and how much shallow geothermal energy can be exploited may well depends on how much temperature drop can be tolerated at the boundary of the next neighbour. This conflict can be more frequent in densely populated cities. Considering both constrains from the minimal inflow temperature and the limit on temperature change at the property boundary, the exploitable capacity of the shallow geothermal energy within a limited space should be estimated by the amount of thermal recharge, instead of by the specific heat extraction rate on each BHE. Based on our results, the specific heat extraction rate may have to be scaled down along with the increasing array size, in order to sustain the long-term operation. This is a very interesting topic that needs to be further investigated in the future.

6.3. pipeline network design

Compared to the analytical approach from You et al. [28], the numerical model presented here has some advantages. Firstly, the seasonal ground surface temperature variation and the vertical geothermal gradient can be accurately quantified. Secondly, the numerical model is able to consider pipeline network with arbitrary connections. Within the pipeline network, the loss of hydraulic head due to friction is automatically computed based on the mass and energy conservation (see section 2.2). Therefore the newly extended model could easily handle a complicated time-dependent hydraulic states within the entire closed-loop system according to different system operation strategy [46, 47]. In addition, a temperature dependent heat pump efficiency curve and pressure-flow rate relationship of the hydraulic pump can also be added into TESPy as input parameters. With such information at hand, electricity consumption due to pump operation can be estimated as soon as the design of the system is available.

As showed in section 3.2, the simulated heat extraction rate on individual BHE will deviate from the designed average value due to the cold thermal plume generated over the long-term operation. This process leads to the different outflow temperature based on the location of the BHE. However, because the BHEs are connected in a parallel way, circulating fluid with higher or lower temperatures will merge together and flows through the heat pump. Then in the next circulation, same inflow temperature will be provided to each BHE. With the parallel setup, the pipe network itself has an intrinsic feature of re-balancing the thermal load among different BHEs. With a higher load from the building, the BHE array responded with a uniform lower inflow and outflow temperature to draw more heat from the subsurface. In Fig. 10, this is demonstrated by the data points moving from the upper-left towards the lower-right corner. Yet, the distribution of load is not homogeneous among the BHEs. With those located at the edge in a better position of extracting heat from the surrounding soil, they also supply a large proportion of the heat.

It should be noticed that the presented pipeline network in this study has an intrinsic feature of re-balancing the thermal load among the BHEs, as it has a fully parallel structure. If the topology of the BHE array is different, the system may show an entirely different behaviour. For example, the connecting pipe may be routed to extract the shallow geothermal energy from BHEs at the periphery first, and using the BHEs in the centre only when the peak load is needed [46]. This opens new opportunities in future research to optimise the connectivity of BHEs in its designing phase. This is already under our investigation and will be presented in a separate manuscript.

7. Conclusion and outlook

In this work, a comprehensive numerical model was developed, with the shallow subsurface, the multiple BHEs and the pipe network explicitly quantified in a single modelling framework. Compared to other existing models, the thermal and hydraulic processes in the pipeline network was explicitly quantified to reproduce the shifting heat extraction rate caused by the thermal interference among multiple BHEs. It is found that over the long-term operation of a large BHE array, the heat extraction rate in the centre was gradually shifted towards those located at the outer boundary. This phenomenon becomes significant with the increasing number of BHEs installed in the array. Over different seasons in a year, the most intensive shifting phenomenon was observed in the lowest thermal demand month. In comparison, the percentage of shifted load reaches its maximum in the month with the lowest thermal load.

As a result, the application of super-positioned infinite line source model with a constant heat flux is considered to be inaccurate for long-term and high thermal load applications. The numerical experiments in this work showed that such analytical approach will lead to an over-estimation in the reduction of soil temperature, as the subsurface recharge process was ignored. In this study a relatively low specific heat extraction rate (maximum 12.5 W/m) was observed on each BHE. However, a maximum 2.5 °C soil temperature difference after 10 years was already been identified by comparing the analytical and our numerical result. It is also found that the soil temperature deviation between the models with or without considering the shifting of thermal load is very limited (<0.5°C), when the specific heat extraction rate is relatively low as demonstrated in this study.

Currently, for simulating of GSHP system especially installed with a large number of BHEs in the array, the method described in this study still exists its shortcomings. A main shortcoming point to the slower computational time, since there are two computing processes (in OGS and in TESPy) within one timestep. In order to alleviate the long simulation time, our group are working on the parallelization of OGS-TESPy code, which may greatly accelerate the speed of simulation.

Acknowledgements

This study is supported by the National Natural Science Foundation of China (grant 41628203). Funding for the project was also provided by the German Federal Ministry of Economic Affairs and Energy (BMWi) under Grant No. 03ET6122B ("ANGUS II: Impacts of the use of the geological subsurface for thermal, electrical or material energy storage in the context of transition to renewable energy sources—Integration of subsurface storage technologies into the energy system transformation using the example of Schleswig-Holstein as a model area") and is gratefully acknowledged. We would like to express our thanks also to our ANGUS II colleagues for the fruitful scientific collaboration and the project lead and management.

References

[1] OECD/IEA, Heating without global warming, Technical Report, International Energy Agency, France, 2014.

[2] IRENA, Geothermal Power: Technology Brief, Technical Report September, International Renewable Energy Agency, Abu Dhabi, 2017. ISBN: 9789292600365.

[3] J. W. Lund, T. L. Boyd, Geothermics Direct utilization of geothermal energy 2015 worldwide review, Geothermics 60 (2016) 66–93. doi:10.1016/j.geothermics.2015.11.004.

[4] T. Kurevija, D. Vulin, V. Krapec, Effect of borehole array geometry and thermal interferences on geothermal heat pump system, Energy Conversion and Management 60 (2012) 134–142. doi:10.1016/j.enconman.2012.02.012.

[5] K. Zhu, P. Blum, G. Ferguson, K.-d. Balke, P. Bayer, The geothermal potential of urban heat islands, Environmental Research Letters 5 (2010) 6pp. doi:10.1088/1748-9326/5/4/044002.

[6] J. A. Rivera, P. Blum, P. Bayer, Increased ground temperatures in urban areas: Estimation of the technical geothermal potential, Renewable Energy 103(C) (2016) 388–400. doi:10.1016/j.renene.2016.11.005.

[7] P. Bayer, G. Attard, P. Blum, K. Menberg, The geothermal potential of cities, Renewable and Sustainable Energy Reviews 106 (2019) 17–30. doi:10.1016/j.rser.2019.02.019.

[8] P. Eskilson, Thermal Analysis of Heat Extraction Boreholes, Ph.D. thesis, University of Lund, Sweden, 1987.

[9] M. A. Bernier, P. Pinel, R. Labib, R. Paillot, A multiple load aggregation algorithm for annual hourly simulations of gchp systems, HVAC&R Research 10 (2004) 471–487. doi:10.1080/10789669.2004.10391115.

[10] L. Lamarche, B. Beauchamp, A new contribution to the finite line-source model for geothermal boreholes, Energy and Buildings 39 (2007) 188–198. doi:10.1016/j.enbuild.2006.06.003.

[11] S. Koohi-fayegh, M. A. Rosen, Examination of thermal interaction of multiple vertical ground heat exchangers, Applied Energy 97 (2012) 962–969. doi:10.1016/j.apenergy.2012.02.018.

[12] S. Koohi-Fayegh, M. A. Rosen, An analytical approach to evaluating the effect of thermal interaction of geothermal heat exchangers on ground heat pump efficiency, Energy Conversion and Management 78 (2014) 184–192. doi:10.1016/j.enconman.2013.09.064.

[13] H. Qian, Y. Wang, Energy for Sustainable Development Modeling the interactions between the performance of ground source heat pumps and soil temperature variations, Energy for Sustainable Development 23 (2014) 115–121. doi:10.1016/j.esd.2014.08.004.

[14] J. A. Rivera, P. Blum, P. Bayer, Influence of spatially variable ground heat flux on closed-loop geothermal systems : Line source model with nonhomogeneous Cauchy-type top boundary conditions, Applied Energy 180 (2016) 572–585. doi:10.1016/j.apenergy.2016.06.074.

[15] P. Bayer, M. de Paly, M. Beck, Strategic optimization of borehole heat exchanger field for seasonal geothermal heating and cooling, Applied Energy 136 (2014) 445–453. doi:10.1016/j.apenergy.2014.09.029.

[16] C. Zhang, Y. Wang, Y. Liu, X. Kong, Q. Wang, Computational methods for ground thermal response of multiple borehole heat exchangers : A review, Renewable Energy 127(C) (2018) 461–473. doi:10.1016/j.renene.2018.04.083.

[17] G. Hellström, Ground heat storage : thermal analyses of duct storage systems, Ph.D. thesis, Lunds University, Sweden, 1991.

[18] B. Morrone, G. Coppola, V. Raucci, Energy and economic savings using geothermal heat pumps in different climates, Energy Conversion and Management 88 (2014) 189–198. doi:10.1016/j.enconman.2014.08.007.

[19] D. Pahud, A. Fromentin, PILESIM : a simulation tool for pile and borehole heat exchanger systems, Bulletin d'Hydrogblogie 17 (1999). URL: https://www.geothermal-energy.org/pdf/IGAstandard/EGC/1999/Pahud.pdf.

[20] C. K. Lee, H. N. Lam, A simplified model of energy pile for ground-source heat pump systems, Energy 55 (2013) 838–845. doi:10.1016/j.energy.2013.03.077.

[21] P. Hein, K. Zhu, A. Bucher, O. Kolditz, Z. Pang, H. Shao, Quantification of exploitable shallow geothermal energy by using Borehole Heat Exchanger coupled Ground Source Heat Pump systems, Energy Conversion and Management 127 (2016) 80–89. doi:10.1016/j.enconman.2016.08.097.

[22] M. Saaly, P. Maghoul, M. Kavgic, D. Polyzois, Performance analysis of a proposed geothermal pile system for heating and cooling energy demand for a building in cold regions, Sustainable Cities and Society 45 (2019) 669–682. doi:10.1016/j.scs.2018.12.014.

[23] COMSOL, Introduction to COMSOL Multiphysics, 2018. URL: https://www.comsol.de/documentation.

[24] B. Hénault, P. Pasquier, M. Kummert, Financial optimization and design of hybrid ground-coupled heat pump systems, Applied Thermal Engineering 93 (2016) 72–82. doi:10.1016/j.applthermaleng.2015.09.088.

[25] S. Kavanaugh, K. Raffert, Ground source heat pumps. Design of geothermal systems for commercial and institutional buildings, ASHRAE, USA, 2014. ISBN: 9781936504855.

[26] A. Gultekin, M. Aydin, A. Sisman, E ff ects of arrangement geometry and number of boreholes on thermal interaction coe ffi cient of multi-borehole heat exchangers, Applied Energy 237 (2019) 163–170. doi:10.1016/j.apenergy.2019.01.027.

[27] H. J. L. Witte, A Novel Tool for Assessing Negative Temperature Interactions between Neighbouring Borehole Heat Exchanger Systems, 14th International Conference on Energy Storage, Adana, Turkey, 2018.

[28] T. You, X. Li, S. Cao, H. Yang, Soil thermal imbalance of ground source heat pump systems with spiral-coil energy pile groups under seepage conditions and various influential factors, Energy Conversion and Management 178 (2018) 123–136. doi:10.1016/j.enconman.2018.10.027.

[29] J. Xi, Y. Li, M. Liu, R. Z. Wang, Study on the thermal effect of the ground heat exchanger of GSHP in the eastern China area, Energy 141 (2017) 56–65. doi:10.1016/j.energy.2017.09.060.

[30] P. Hein, O. Kolditz, U. J. Görke, A. Bucher, H. Shao, A numerical study on the sustainability and efficiency of borehole heat exchanger coupled ground source heat pump systems, Applied Thermal Engineering 100 (2016) 421–433. doi:10.1016/j.applthermaleng.2016.02.039.

[31] C. Chen, H. Shao, D. Naumov, Y. Kong, K. Tu, O. Kolditz, Numerical investigation on the performance, sustainability, and efficiency of the deep borehole heat exchanger system for building heating, Geothermal Energy 7 (2019) 18. doi:10.1186/s40517-019-0133-8.

[32] S. Miglani, K. Orehounig, J. Carmeliet, A methodology to calculate long-term shallow geothermal energy potential for an urban neighbourhood, Energy & Buildings 159 (2017) 462–473. doi:10.1016/j.enbuild.2017.10.100.

[33] Energy Saving Trust, Domestic ground source heat pumps: Design and installation of closed-loop systems – a guide for specifiers, their advisors and potential users, The Energy Saving Trust Report CE82, London, 2007.

[34] The Association of German Engineers(Verein Deutscher Ingenieure), Thermische nutzung des untergrunds erdgekoppelte waermepumpenanlagen; vdi 4640, blatt 2, Beuth Verlag GmbH, Berlin, 2001.

[35] The Association of German Engineers(Verein Deutscher Ingenieure), Thermal use of the underground ground source heat pump systems; vdi 4640, blatt 2, entwurf, VDI-Gesellschaft Energie und Umwelt, 2015.

[36] GB50366, Technical code for ground-source heat pump system, Ministry of Housing and Urban-Rural Development, PR China, 2009.

[37] H.-J. J. G. Diersch, D. Bauer, W. Heidemann, W. Rühaak, P. Schätzl, Finite element modeling of borehole heat exchanger systems: Part 1. Fundamentals, Computers & Geosciences 37 (2011) 1122–1135. doi:10.1016/j.cageo.2010.08.003.

[38] F. Witte, Thermal engineering systems in python, 2019. URL: https://doi.org/10.5281/zenodo.2555866. doi:10.5281/zenodo.2555866.

[39] L. Böswirth, S. Bschorer, Technische Strömungslehre, Springer Fachmedien Wiesbaden, 2014. doi:10.1007/978-3-658-05668-1.

[40] I. H. Bell, J. Wronski, S. Quoilin, V. Lemort, Pure and pseudo-pure fluid thermophysical property evaluation and the open-source thermophysical property library coolprop, Industrial & Engineering Chemistry Research 53 (2014) 2498–2508. doi:10.1021/ie4033999. arXiv:http://pubs.acs.org/doi/pdf/10.1021/ie4033999.

[41] O. Kolditz, S. Bauer, L. Bilke, et al., OpenGeoSys: an open-source initiative for numerical simulation of thermo-hydro-mechanical/chemical (THM/C) processes in porous media, Environmental Earth Sciences 67 (2012) 589–599. doi:https://doi.org/10.1007/s12665-012-1546-x.

[42] L. a. Rossman, EPANET 2: users manual, Cincinnati US Environmental Protection Agency National Risk Management Research Laboratory 38 (2000) 200. doi:10.1177/0306312708089715.

[43] M. Richter, C. Huber, K. Reinhardt, H. Wachmann, A. Gerschel, Potential of heat supply for saxon gardening companies utilizing geothermal energy as subject to site-specific geological conditions and different business organisations/ utilisation concepts (Möglichkeiten der Wärmeversorgung von sächsischen Gartenbaubetrieben mit Geothermie in abhängigkeit von geologischen Standortfaktoren und verschiedenen Betriebsstrukturen/Nutzungskonzepten), 2015.

[44] A. Gultekin, M. Aydin, A. Sisman, Thermal performance analysis of multiple borehole heat exchangers, Energy Conversion and Management 122 (2016) 544–551. doi:10.1016/j.enconman.2016.05.086.

[45] T. You, W. Wu, W. Shi, B. Wang, X. Li, An overview of the problems and solutions of soil thermal imbalance of ground-coupled heat pumps in cold regions An overview of the problems and solutions of soil thermal imbalance of ground-coupled heat pumps in cold regions, Applied Energy 177 (2016) 515–536. doi:10.1016/j.apenergy.2016.05.115.

[46] H. M. Haq, E. Hiltunen, An inquiry of ground heat storage: Analysis of experimental measurements and optimization of system's performance, Applied Thermal Engineering 148 (2019) 10–21. doi:10.1016/j.applthermaleng.2018.11.029.

[47] K. W. Tordrup, S. E. Poulsen, H. Bjørn, An improved method for upscaling borehole thermal energy storage using inverse finite element modelling, Renewable Energy 105 (2017) 13–21. doi:10.1016/j.renene.2016.12.011.